Divergent biological response to neoadjuvant chemotherapy in muscle-invasive bladder cancer

Running title: Classification of bladder cancer not responding to cisplatin

Roland Seiler[123#], Ewan A. Gibb[3#], Natalie Q. Wang[3], Htoo Zarni Oo[1], Hung-Ming Lam[4], Kim E. van Kessel[5], Charlotte S. Voskuilen[6], Brian Winters[4], Mandeep Takhar[3], Nicholas Erho[3], James Douglas[7], Funda Vakar-Lopez[4], Simon J. Crabb[8], Bas W.G. van Rhijn[6], Elisabeth E. Fransen van de Putte[6], Ellen C. Zwarthoff[5], George N. Thalmann[2], Elai Davicioni[3], Joost L. Boormans[9], Marc Dall'Era[10], Michiel S. van der Heijden[8], Jonathan L. Wright[4] and Peter C. Black[1]

[1] Department of Urologic Sciences, University of British Columbia, Vancouver, British Columbia, Canada
[2] Department of Urology, University of Bern, Bern, Switzerland
[3] GenomeDx Biosciences, Inc., Vancouver, British Columbia, Canada
[4] Department of Urology, University of Washington School of Medicine, Seattle, Washington, USA
[5] Department of Pathology, Erasmus MC, University Medical Center Rotterdam, Rotterdam, The Netherlands
[6] Department of Surgical Oncology, Division of Urology, Netherlands Cancer Institute – Antoni van Leeuwenhoek Hospital, Amsterdam, The Netherlands
[7] Department of Urology, University Hospital of Southampton, Hampshire SO16 6YD, UK
[8] Department of Medical Oncology, University Hospital of Southampton, Hampshire SO16 6YD, UK
[9]Department of Urology, Erasmus MC Cancer Institute, Rotterdam, The Netherlands
[10]UC Davis Comprehensive Cancer Center, Sacramento, CA 95817, USA (MD)

[#] Contributed equally

Keywords: Muscle-invasive bladder cancer; neoadjuvant chemotherapy; cisplatin-resistance; second-line treatment; molecular subtypes; gene expression analysis

Address correspondence to:
Roland Seiler, MD
Department of Urology
University of Bern
Bern 3010, Switzerland
r_seiler@gmx.ch

Conflict of interest:
Each author has made a substantial contribution to the article and have read and approved the final, submitted manuscript. Of these, five authors (EG, NW, MT, NE, ED) are employees of GenomeDx Biosciences, which funded the original gene expression analysis of the patient tissue and assisted with data analysis. The remaining authors have no direct or indirect commercial financial incentive associated with publishing the article. The first author's (RS) salary was funded by the Swiss National Foundation and by GenomeDx. The manuscript or portions thereof are not under consideration by another journal or electronic publication and have not been previously published.

Statement of Significance (149 words)

Despite cisplatin-based neoadjuvant chemotherapy (NAC) 60% of patients with muscle-invasive bladder cancer still have residual invasive disease at radical cystectomy (RC). The NAC-induced biological alterations in these cisplatin-resistant tumors remain largely unstudied. We analyzed gene expression from 116 matched pairs pre- and post-NAC. H&E and immunohistochemistry were used to confirm tissue sampling and gene expression analysis. Established molecular subtyping models proved to be inconsistent in their classification of the post-NAC samples. Unsupervised consensus clustering revealed four distinct consensus clusters (CC). The CC1-Basal and CC2-Luminal subtypes expressed genes consistent with a basal-like and a luminal-like phenotype, respectively. The CC3-Immune subtype had the highest immune activity, including T-cell infiltration and checkpoint molecule expression, but lacked both basal and luminal markers. The CC4-Scar-like subtype expressed genes associated with wound-healing/ scarring and was associated with favorable prognosis. Further evaluation is necessary to determine if this subtyping could impact the selection of second-line treatment.

ABSTRACT (244 words)

Purpose: After cisplatin-based neoadjuvant chemotherapy (NAC) 60% of patients with muscle-invasive bladder cancer still have residual invasive disease at radical cystectomy (RC). The NAC-induced biological alterations in these cisplatin-resistant tumors remain largely unstudied.
Experimental Design: RC samples were available for gene expression analysis from 133 patients with residual invasive disease after cisplatin-based NAC, of whom 116 had matched pre-NAC samples. Unsupervised consensus clustering (CC) was performed and the CC were investigated for their biological and clinical characteristics. H&E and immunohistochemistry on tissue microarrays were used to confirm tissue sampling and gene expression analysis.
Results: Established molecular subtyping models proved to be inconsistent in their classification of the post-NAC samples. Unsupervised consensus clustering revealed four distinct consensus clusters (CC). The CC1-Basal and CC2-Luminal subtypes expressed genes consistent with a basal and a luminal phenotype, respectively, and were similar to the corresponding established pre-treatment molecular subtypes. The CC3-Immune subtype had the highest immune activity, including T-cell infiltration and checkpoint molecule expression, but lacked both basal and luminal markers. The CC4-Scar-like subtype expressed genes associated with wound-healing/ scarring, although the proportion of tumor cell content in this subtype did not differ from the other subtypes. Patients with CC4-Scar-like tumors had the most favorable prognosis.
Conclusion: This study expands our knowledge on muscle-invasive bladder cancer not responding to cisplatin by suggesting molecular subtypes to understand the biology of these tumors. Although these molecular subtypes imply consequences for adjuvant treatments, this ultimately needs to be tested in clinical trials.

INTRODUCTION

Muscle-invasive bladder cancer (MIBC) is an aggressive malignancy associated with a 50% mortality rate at 5 years (1, 2). Optimal treatment consists of neoadjuvant cisplatin-based chemotherapy (NAC) followed by radical cystectomy (RC). While NAC has been shown to improve the overall survival rate by 5-7%, in the real-world setting only ~40% of patients experience a major response, as defined by having no residual MIBC in the RC specimen (3). Persistent invasive bladder cancer after NAC is considered chemoresistant (3), and patients with residual cancer at RC are at a high risk for disease progression (4).

Gene expression-based molecular subtyping of chemotherapy-naïve MIBC has advanced our understanding of this heterogeneous disease (5-10). Response to NAC or immunotherapy, especially checkpoint blockade, has been shown to correlate with molecular subtype (8, 11-14). However, platinum-based chemotherapy and immunotherapy are highly likely to shift the biological and clinical behavior of a tumor, which would be expected to impact molecular subtyping.

Molecular alterations induced by chemotherapy are poorly characterized, but early evidence suggests that significant alterations occur at the level of both the genome and transcriptome. For example, chemotherapy has been shown to affect the clonal evolution of an individual patient's tumor (15). An early study on molecular subtypes suggested that NAC may induce subtype switching (8), indicating that NAC induces phenotypical changes on the transcriptome level, or selects one subtype over another in a mixed, heterogeneous tumor.

In this study, we assembled a large dataset of residual invasive bladder cancer after NAC and investigated these tumors using transcriptome-wide gene expression and immunohistochemistry for the molecular characterization of cisplatin-resistant bladder cancer.

MATERIALS AND METHODS

Patients

A consecutive cohort of MIBC patients from seven institutions was enrolled. All patients were treated with curative intent. After initial diagnosis of MIBC by transurethral bladder tumor resection (TURBT), each patient received at least three cycles of cisplatin-based NAC followed by RC. After completion of consensus clustering it was recognized that one patient had been treated with carboplatin-based NAC. Although, this patient was included for consensus clustering, it was removed for all subsequent analysis. Briefly, this cohort included 295 TURBT and 144 RC specimens. After quality control filtering (see below) 134 patients with post-NAC gene expression profiles were available for analysis **(Table S1**), for subsequent analysis, 133 patients were included after removal of the case treated with carboplatin. In addition, a total of 21 non-neoplastic scar tissue samples were collected from the tumor-bed of RC specimens with a complete pathological response (pT0N0).
The human ethics board of each institution approved this study and all patients consented to analysis of their tumor tissues. Protocol numbers: Bern, Switzerland KEK-Be 219/2015; Vancouver, BC, Canada H09-01628; Southampton, UK, 10/H0405/99; Seattle, Washington, USA, FHCRC: #7116; Amsterdam, the Netherlands, CFMPB-104; UC Davis, Sacramento, USA, 438935-6; Rotterdam, the Netherlands, MEC-2014-642. This research was carried out in accordance with the approved guidelines.

Tissue sampling and gene expression profiling

Whole transcriptome analysis was performed on formalin-fixed, paraffin-embedded tumor tissue with GeneChip® Human Exon 1.0 ST Array (Affymetrix) in a Clinical Laboratory Improvement Amendments (CLIA)-certified laboratory (16). 134/144 post-NAC samples and 21/21 scar samples passed quality control, respectively. Microarray data from the corresponding pre-NAC samples were taken from our previously published dataset (14). For subsequent analysis, the patient treated with carboplatin was excluded and only 133 samples were used. Microarray data surpassing all quality measures were available for matched pairs of pre- and post-NAC samples from 116 patients, all of whom received cisplatin-based NAC. Microarray data were normalized and genes summarized using single-channel array normalization (17).

Unsupervised consensus clustering

Unsupervised consensus clustering was performed using the ConsensusClusterPlus (18) package in R (R Core Team (2014). Low-varying genes were filtered out by selecting the 2000 genes with the highest median absolute deviation. Bootstrap clustering was performed with 10000 iterations, using Pearson correlation as the similarity metric, and Ward's algorithm for clustering. We focused on two, three and four cluster solutions that showed a sequential separation of each group.

Gene set expression analysis

GSEA software from the public domain (http://www.broad.mit.edu/gsea/) (19) generated enrichment plots and calculated significance of gene signatures. Genes were ranked with Signal2Noise and a weighted enrichment statistic was used to calculate Normalized Enrichment Scores, p-values and false detection rate.

Immunophenotype scoring

The immunophenotyped model was originally developed by Charoentong *et al*, 2017 (20). Using machine learning and the published lists of immune genes, we created a weighted average signature based on the authors published model. This model was then applied to our cohort to generate the immunophenotype scores.

Quantification of tumor for tissue sampling

Tumor content was assessed by two expert investigators (RS, HO) using H&E sections taken from the same tissue blocks sampled for gene expression analysis. Both investigators were blinded to the consensus clusters. For each sample, the percentage of tumor area in relation to the total area of tissue on the section was estimated. The largest coherent tumor focus on the section was measured and within this focus, the percentage of cancer cells in relation to all cells was estimated. For all quantifications, no differences were observed between the estimates of both pathologists ($p>0.05$).

Tumor regression grading

A subset of post-NAC tumors from three centers were classified according to previously published methods into tumor regression grades (TRG; (21)). The TRG were determined previously for a different project and therefore, investigators were blinded to the consensus clusters. TRG was defined by histologic estimation of the size of the residual viable tumor relative to the size of the original tumor bed, which was indicated by zones of fibrosis. TRG 3 and TRG 2 were defined as having ≤50% and >50% tumor regression, respectively. The 21 scar samples were equivalent to TRG 1 (complete tumor regression).

Assignment to subtypes using additional models

Assignment of the pre- and post-NAC samples to the molecular subtypes was performed as previously described (14). Briefly, we used five established subtyping models including the Genomic Subtyping Classifier (GSC) (14). The four other models included the University of North Carolina (UNC) (7, 9), The Cancer Genome Atlas (TCGA) (6), Lund University (Lund 2012) (5), and MD Anderson (MDA) (8).

Construction of tissue microarrays and immunohistochemistry

The tissue microarrays (TMA) were prepared for immunohistochemical (IHC) analysis by taking a maximum of 4 samples per patient. Two were harvested from the primary tumor before NAC (TURBT) and, if still present, two from the residual tumor after NAC (RC). The freshly cut tissue sections/TMAs were used to determine the protein expression of targets of interest.

In brief, the TMAs were incubated in buffer (Tris-EDTA (cell conditioning 1: CC1) at 95°C for 60 minutes, followed by incubation with primary antibody at 37°C for 60 minutes. The following antibodies were used: PPARy (anti-rabbit, clone #2435, Cell Signaling Technology, 1:100 dilution (22)), CD8 (anti-mouse, NCL-L-CD8-4B11, Leica, 1:100 dilution (22)), KRT5/6 (anti-mouse, clone #D5/16B, Millipore, 1:400 dilution), GATA3 (anti-mouse, clone #L50-823, Cell Marque, 1:1600 dilution), Ki67 (anti-mouse, clone #M7240, Dako, 1:100 dilution), and CD44 (anti-rabbit, clone #EPR1013Y, Abcam, 1:100 dilution (23)). The TMAs were washed and incubated with Ventana universal secondary antibody at 37°C for 32 min before being visualized

using Ventana DAB Map detection kit. All IHC staining was performed using the Ventana Discovery Ultra autostainer.

When assessing the staining intensity, the nuclear (GATA3, Ki67), cytoplasmic (KRT5/6) and membranous/cytoplasmic (PPARy, CD8, CD44) subcellular localization was taken into consideration. The scoring for GATA3, KRT5/6, PPARy and CD44 was determined using a 4-point scale system as well as percentage of stained cancer cells. Score 0 represents no staining or absence of any tumor cells, score 1 represents a weak stain, score 2 represents a moderate intensity stain and score 3 is a strong stain. The overall protein expression was determined by multiplying the intensity score by the percentage. For Ki67, the percentage of stained cancer cells in relation to all cancer cells was considered. For CD8, the number of CD8 positive tumor infiltrating cells were counted in each tissue core. For all staining, the average of two cores was used for further analysis.

Statistical analyses

All statistical analyses were conducted using R version 3.3.3. All tests of significance were two-sided at 0.05 level.

In order to measure concordance between subtyping models, we compared the GSC to four published classification methods: UNC, MDA, The Cancer Genome Atlas (TCGA), and Lund University (Lund). The subtypes in each model were given a basal or luminal call as follows. Luminal included UNC Luminal; TCGA Cluster I and II; MDA Luminal; Lund Genomically Unstable and UroA; and GSC Luminal and Luminal Infiltrated. Basal included: UNC Basal and Claudin-low; TCGA Cluster III and IV; MDA Basal; Lund SCC-like and UroB; and GSC Basal and Claudin-low. The Lund Infiltrated and MDA p53-like subtypes were considered neutral. Concordance (agreement) was then calculated as the absolute value of difference between the number of Luminal votes and the number of Basal votes. If there was a tie between Luminal and Basal, the concordance was given assigned a 0.

Kaplan-Meier curves were used to show overall survival stratified by subtype according to each classification scheme (GSC model, UNC, TCGA, MDA, Lund and the unsupervised consensus clusters). Log-rank tests were used to compare event rates between the subtyping groups, while Cox proportional models were used to evaluate the importance of consensus clustering for prediction of overall survival. Subtyping calls before and after NAC were compared using a chi-squared test. For statistical tests comparing pre- and post-NAC samples, we used 116 patients. For statistical tests focused exclusively on the post-NAC setting, 133 patients who received RC after cisplatin-based NAC were used. For all the analyses associated with survival time, two patients were excluded because of missing data.

RESULTS

Patient characteristics

The clinical and pathological features of the patient cohort are described in Table S1. The median age of the 134 patients (38 females, 96 males) at surgery was 61 years. During a median follow-up of 35.4 months, 62 and 56 patients had cancer recurrence and died, respectively. Because patients in this retrospective cohort were treated before the immune checkpoint era, none of the patients in this cohort received immune checkpoint blockade. A variety of agents were used in different combinations as second-line treatments which was most often initiated after cancer recurrence. There was no difference in the use of second-line treatments or chemotherapy regimens between different post-NAC subtypes.

Molecular subtyping of bladder cancer after cisplatin-based neoadjuvant chemotherapy

Subtype calls were generated for a matched (pre-/post-NAC) MIBC patient cohort (n=116) by applying our single-sample genomic subtyping classifier (GSC) (14) (**Figure 1**) and other published subtyping models to these data (5-9) (**Figure S1**). Survival analysis showed that only the GSC model was prognostic in this cohort (**Figure 1A**). We found patients with basal or luminal tumors had a favorable prognosis compared to patients with claudin-low or luminal-infiltrated tumors, when analyzed before (TURBT) and after (RC) NAC ($p<0.05$; **Figure 1A & 1B**). Notably, the MD Anderson (MDA) p53-like and Lund Infiltrated subtypes both showed a shift towards a favorable prognosis in post-NAC RC samples (**Figure S2D & S2H**).

We also observed a marked shift in the distribution of subtypes after NAC (**Figure 1C & Figure S1**), with the post-NAC subtype varying frequently from the pre-NAC subtype. When comparing the subtype calls for all models, we found a general agreement between pre-NAC subtype calls in TURBT samples consistent with our previous report (14) (**Figure 1D**, left panel). However, in the post-NAC RC setting we observed fewer luminal subtype calls and an enrichment of basal, p53-like and infiltrated subtypes (**Figure 1D**, right panel). We observed a loss of concordance with respect to the basal/luminal axis, with higher model agreement in pre-NAC samples (Fleiss' Kappa 0.49) than in post-NAC samples (Fleiss' Kappa 0.30, $p<0.001$; **Figure 1E**).

Taken together, these results highlight that molecular subtyping can provide prognostic information both before and after chemotherapy, but the classification of MIBC using these models will change after exposure to NAC.

Cisplatin-resistant bladder cancer can be classified into four distinct biological subtypes

Current evidence suggests cisplatin-based therapies can drive the evolution of bladder tumors by inducing genomic alterations and / or by selecting for cisplatin-resistant clones within a molecularly heterogeneous tumor (8, 15). We therefore hypothesized that the relative shift in the distribution of subtypes in the post-NAC setting was a consequence of cisplatin-induced or cisplatin-selected changes in the biological and genomic characteristics of the cisplatin-resistant tumors (defined as $ypT \geq 2$ or $ypN \geq 1$).

To test this hypothesis, we employed unsupervised consensus clustering (CC) with a subset of highly variant genes and identified a robust 4-cluster solution (**Figure S3**). Importantly, CC using different input gene sets identified essentially the same classes (**Table S2, Figure S3**). An investigation of the biological characteristics of the individual clusters revealed that CC1 and

CC2 were consistent with established basal and luminal MIBC molecular subtypes (**Figure 2**). The CC1 tumors tended to have higher expression of basal-associated genes (i.e. *KRT5, KRT14, CD44*; **Figure 2A & 2B**), while the CC2 tumors had higher expression luminal-associated genes (i.e. *KRT20, PPARG, GATA3*; **Figure 2A & 2C**).

To confirm the cluster assignment on the basal and luminal axis, tissue microarrays (TMAs) were stained with basal (KRT5/6 and CD44) and luminal (GATA3 and PPARγ) markers (**Figure 2D**-**F**). Importantly, two different areas of each tumor correlated strongly between matched cores (R=0.91, **Figure S4**). As expected, tumors in CC1 showed higher protein expression of KRT5/6 and CD44 (**Figure 2E**), whereas the protein expression of GATA3 and PPARγ (**Figure 2F**) was low. The opposite pattern was observed for tumors in CC2, which showed high protein expression for GATA3 and PPARγ (**Figure 2F**) and low expression of basal markers (**Figure 2E**). Given these data, we named these subtypes CC1-Basal and CC2-Luminal.

Immune signaling defines the biology of one group of cisplatin-resistant tumors

Higher expression of immune-associated genes (i.e. *CTLA4*, *MPEG1* and *CD27*) was noted in both the CC1-Basal and CC3, with lower expression in CC4 and little in the CC2-Luminal (**Figure 2A & Figure S5**). However, CC3 lacked robust expression of basal or luminal markers which defined CC1-Basal and CC2-Luminal, respectively.

To explore the immunological activity of CC3, we applied two different immune signatures to the four clusters. First, we found that the expression patterns of genes from the Pan Cancer Immune Profiling Panel (24), were significantly higher in CC3 compared to the other clusters (**Figure 3A**, p=0.01, NES=1.88). A second immune signature (immune 190 (22)) showed low scores for the CC2-Luminal subtype, with higher scores associated with the CC3 and the CC1-Basal subtype (**Figure 3B**).

As T-cell infiltration can significantly impact the tumor microenvironment, we hypothesized the higher immune scores may be related in part to T-cell activity. Consistent with this hypothesis, we found higher T-cell and T-helper cell signature scores in the immune infiltrated clusters, with the highest scores in CC3 and the lowest in CC2-Luminal (**Figure 3C & 3D**). These findings were confirmed with IHC, where particularly high T-cell infiltration was observed in CC3 and almost none in CC2-Luminal (**Figure 3E & 3F**).

Interestingly, high PPARγ expression (**Figure 2**) and lower immune activity observed in the CC2-Luminal subtype provide supporting evidence that *PPARG* activity can create an immune-deficient tumor environment in MIBC, even in the post-NAC setting (22). Moreover, CC1-Basal and CC3 not only had higher immune signature scores, but also showed higher expression of the immune suppressor genes *PD-L1*, *PD-L2* and *CTLA4*, suggesting an immune-suppressive microenvironment (**Figure S5**).

Finally, we also determined that the enrichment of immune activity observed for CC3 was not exclusively driven by T-cells, as this cluster also robustly expressed many chemokines and cytokines (**Figure 3G**, p=0.018, NES=1.77). Collectively, due to the lack of basal or luminal marker expression and the higher level of immune cell infiltration and signaling, we named this subtype CC3-Immune.

Wound-healing and scar-like characteristics define the biology of a group of cisplatin-resistant tumors

Many of the highly-expressed genes in CC4 were associated with the p53-like signature described in the MDA classifier (8, 25) (**Figure 2A**). We also found higher expression of genes that were consistent with wound healing/scarring (*MYH11, CNN1, DES*) or with epithelial-to-mesenchymal transition (EMT; i.e. *ZEB1, ZEB2, VIM*), suggesting these patients had response to therapy (**Figure 2A, Figure S6**).

Histological examination of these patient tumors revealed significant tumor content, confirming these patients were in fact pathological non-responders (**Figure 4A, Figure S7**). The CC1-Basal tumors had the largest tumor diameter (**Figure S7A, S7B**), however the median percentage of tumor cells in the sampled tumor area was above 60% in all four clusters (**Figure S7C**). The presence of tumor cells was also confirmed with KI67 IHC, where marked staining was observed in samples from all four clusters (**Figure 4B & 4C**). Interestingly, a cell cycle gene signature showed lower proliferation for CC4 tumors, suggesting these tumors may be more quiescent (**Figure 4D**). The area of tumor sampled contained a similar proportion of stromal elements between all four CC (**Figure S7**), nonetheless we found additional gene signatures that supported a scar-like phenotype (**Figure 4E**).

When we compared the CC4 tumors to tissue sampled from the tumor bed (non-neoplastic scar tissue in RC sample) of patient who had a complete response to NAC (i.e. pT0N0), we found highly consistent gene expression signatures (**Figure 4F**). Using principle component analysis (PCA), we found CC4 tended to separate with true scar tissues and away from CC1-CC3 tumors on PC1, but grouped with the tumor samples on PC2 (**Figure 4G,** left panel). On PC3 we observed a distinct separation of the CC1-Basal and CC2-Luminal tumors, with minimal separation of CC3 and CC4 (**Figure 4G,** right panel). Collectively, the three PCs tended to separate the CC1-CC3 tumors from the CC4 and scar tissues, which clustered together (**Figure S8, Table S3)**. These data indicate that the CC4 and scar tissues share similar genomic profiles.

To determine whether there was an association between the CC and prognosis, we performed a survival analysis. This revealed that CC4 has a favorable prognosis compared to CC1-CC3 in the Kaplan Meier plot (**Figure 4H**) but was not associated with lower tumor stages at RC (**Figure S9**). In a univariable analysis, the relative risk in CC4-Scar-like was 2.8 times less than CC2-Luminal (HR=0.36, p=0.038), and 3 times less than CC3-Infiltrated (HR=0.33, p=0.018) for predicting overall survival (**Table S4**). In a multivariable analysis adjusting for age, stage and nodal status, CC4 had significantly better survival compared to CC3 (HR=0.36, p=0.038) and CC2 (HR=0.38, p=0.071).

We have previously reported on histologically determined tumor regression grades (TRG) after NAC in bladder cancer, and established criteria that define partial responders (TRG 2) within the cohort of patients with residual MIBC after NAC (21). We showed that these partial responders had in improved overall survival compared to non-responders (TRG 3). Here we hypothesized the Scar-like subtype may reflect a gene expression correlate of TRG 2. Analysis of a subset of the patient cohort confirmed that TRG 2 was enriched amongst the Scar-like tumors (**Table S5**, p=0.026).

Matched comparisons: NAC leads to diverse alterations in MIBC

Pair-wise comparison of tumors before and after NAC revealed that approximately 42% (49/116) of tumors remained static with respect to subtype after chemotherapy (**Figure 5**). These tumors were basal (11) / claudin-low (16) or luminal (18) / luminal-infiltrated (4) at TURBT and clustered with the CC1-Basal or CC2-Luminal subtypes, respectively, at RC (**Figure 5**).

The next most conspicuous change after NAC was a loss of luminal and basal marker expression combined with an enrichment for immune infiltration (CC3-Immune), which occurred in 34% (39/116) of cases. Of the pre-NAC luminal tumors, which lacked immune infiltration, 32% (13/41) became immune infiltrated post-NAC. We did not observe the CC3-Immune subtype arising out of any one of the pre-NAC subtypes more than another, which may imply that this is a more generalized immune response associated with chemotherapy-induced cell death (26, 27). In contrast, we found luminal tumors were more likely than basal tumors to become CC4-Scar-like after NAC (12/55 vs. 2/61, p=0.006). In all cases, we observed similar patterns for the other subtyping models used in this study (**Figure S8)**.

DISCUSSION

Until recently, the treatment of MIBC has remained static for years, despite high mortality rates and optimal treatment (1, 2). The era of targeted therapies has up to now bypassed bladder cancer, and cisplatin-based chemotherapy remains a critical component of MIBC therapy. Recent studies have begun to detail NAC responses at a higher resolution, where basal tumors have been shown to benefit the most with respect to overall survival after NAC (14, 28). Specific mutations in ERCC2 and other DNA repair genes also predict for excellent outcomes after NAC (29, 30). In the metastatic setting, immunotherapy has had a major impact on cisplatin-resistant MIBC, with approximately 20% of patients achieving a durable objective response to checkpoint blockade (11, 13). However, alternative second-line treatment options for the other 80% of non-responding patients are lacking (11, 13, 31, 32). Therefore, an improved understanding of cisplatin-resistant MIBC genomics could help identify patients who may benefit from existing or emerging second-line treatments.

In this study, we investigated a large cohort of matched pre- and post-NAC MIBC samples and developed a novel subtyping scheme to define the genomics of cisplatin-resistant MIBC. In the post-NAC setting we identified four distinct subtypes which we named CC1-Basal, CC2-Luminal, CC3-Immune and CC4-Scar-like (**Figure 6**). Notably, the CC1-Basal and CC2-Luminal subtypes were highly consistent with the established chemo-naïve basal and luminal subtypes, respectively. Although cluster assignments using different parameters resulted in similar clustering-solutions, the silhouette widths for CC3-Immune and CC4-Scar-like were wide, suggesting instability, similar to the previous descriptions of treatment-naïve MIBC as “p53-like” or “infiltrated” (5, 8).

After chemotherapy, it is assumed that even cisplatin-resistant tumors will undergo some degree of apoptosis, resulting in chemokine release and immune cell recruitment to the tumor site (33). In both the CC1-Basal and CC3-Immune, we observed an enrichment of immune infiltration and chemokine / cytokine activity consistent with this occurrence. However, these tumor-infiltrating immune cells are likely in a quiescent state given the lack of tumor clearing and higher expression of immunosuppressive genes including checkpoint markers in both the CC1-Basal and CC3-Immune. Patients in the CC3-Immune cluster had the worst prognosis, which indicates both the greatest need and simultaneously the greatest potential benefit from second-line treatments, such as checkpoint inhibition.

The CC4-Scar-like transcriptome profile was highly similar to non-neoplastic scar tissue. This subtype lacked basal or luminal marker expression, but robustly expressed fibrosis and ECM markers, consistent with the wound-healing response which leads to scarring (34). CC4-Scar-like tumors share similarities with the previously described p53-like subtype(8). However, this postNAC stromal / p53-like signature was found to be distinct from preNAC p53-like tumors (8). Work in kidney has shown that damaged epithelial cells can be induced to a partial EMT state, which coincides with a loss of epithelial markers and an arrest of cell cycle activity (35). Given the tumor content in these samples, we hypothesize the gene expression patterns driving this cluster were not only derived from infiltrating fibroblasts, but also from tumor cells that are shifting to a transcriptional program consistent with fibrosis. Dvorak et al. offered the compelling idea that these “scar cancers”, referring to tumors that did not arise in a previously healed wound site (scar), but rather were responsible for generating the desmoplastic stroma in which they are embedded (36). This may be most consistent with our CC4-Scar-like cluster, as these samples still have significant tumor content, but a concurrent robust desmoplastic stromal (p53-like) signature. Alternatively, it is possible that the tumor cells themselves have become quiescent in response to chemotherapy, facilitating the infiltration of fibroblasts and subsequent

‘wound healing’ signature observed in these samples. In truth, it may be something closer to the intersection of these two ideas. Biologically, this may be interpreted as a partial response to NAC and, indeed, the patients in this group seem to have improved prognosis. Finally, these findings also corroborate previously reported histologic tumor regression grades (21).

While an obvious pattern for the shift of subtypes before and after NAC did not emerge, we still made several important observations. We characterized one subtype based on a loss of luminal and basal marker expression with concomitant persistence or gain of marked immune infiltrate after chemotherapy, leaving the immune infiltration as the defining feature of this subtype. Immune infiltration is not unique to this subtype, since the pre-NAC GSC luminal-infiltrated tumors are also defined in part by immune-infiltration, and both basal and claudin-low subtypes also have significant immune infiltration. In the future, a more granular analysis of pre- and post-NAC immune characteristics could focus on qualitative differences in the nature of immune infiltration related to therapy.

We hypothesize that the shift in subtypes after NAC is due to tumor plasticity. However, we acknowledge that some of the shift in subtypes may reflect inherent tumor heterogeneity. Furthermore, it is possible that NAC selects for one subtype over another so that a minor subtype in the TURBT sample becomes the predominant subtype in the RC sample. Thomsen et al. recently reported on intratumoral heterogeneity in 4 patients with MIBC. Both basal and luminal clones were present in two cases with multifocal disease (one patient had both MIBC and non-MIBC), but the subtyping was uniform in the other two cases with unifocal MIBC (37). Other reports have suggested that multiple MIBC clones have highly consistent gene expression profiles (38). In the current analyses, there was close correlation in IHC staining between different tumor areas. Furthermore, the shift of approximately 40% of cases to two different subtypes (CC3 and CC4) that were not observed in the pre-NAC setting would imply that the changes are due at least in large part to real changes in biology and not necessarily tumor heterogeneity.

We acknowledge several other potential confounders in our analysis. First, this study is limited by its retrospective nature and the limited sample size of our dataset. In addition, there is a potential for gene expression profiles to vary between TURBT and RC samples (39). It is possible that some differences in gene expression are not only due to NAC but may reflect a wound-healing reaction in response to TURBT. Finally, although the majority of patients in this study had a single tumor, we cannot exclude that multifocality was present in a small number of cases, and that different tumor sites were sampled at TURBT and RC in some cases.

This study advances our understanding of the biology of cisplatin-resistant MIBC and allows us to speculate about the potential implications for post-chemo treatment options. Critically, we have shown that there are two unique immune-infiltrated subtypes (CC1-Basal and CC3-Immune). It will be important to determine in future studies whether these two subtypes will respond differentially to subsequent immunotherapy. The unfavorable outcome of CC2-Luminal tumors suggests that targeted therapies may be most important for these tumors (40). On the other hand, further treatment may not be necessary in CC4-Scar-like tumors, which showed a favorable outcome after NAC and RC, despite a lack of complete pathological response. Prospective clinical trials will be necessary to determine the benefit of specific adjuvant or salvage treatments in each tumor class in order for this work to gain clinical utility.

ACKNOWLEDGEMENTS

- Patients and patient families
- Funding
    - RS – Salary funded by the Swiss National Foundation and partly by GenomeDx.
    - GenomeDx funded gene expression analysis.
    - Five authors (EG, NW, MT, NE, ED) are employees of GenomeDx Biosciences.

REFERENCES

1. Alfred Witjes J, Lebret T, Comperat EM, Cowan NC, De Santis M, Bruins HM, et al. Updated 2016 EAU Guidelines on Muscle-invasive and Metastatic Bladder Cancer. Eur Urol. 2017;71(3):462-75.
2. Stein JP, Lieskovsky G, Cote R, Groshen S, Feng AC, Boyd S, et al. Radical cystectomy in the treatment of invasive bladder cancer: long-term results in 1,054 patients. J Clin Oncol. 2001;19(3):666-75.
3. Zargar H, Espiritu PN, Fairey AS, Mertens LS, Dinney CP, Mir MC, et al. Multicenter assessment of neoadjuvant chemotherapy for muscle-invasive bladder cancer. Eur Urol. 2015;67(2):241-9.
4. Bhindi B, Frank I, Mason RJ, Tarrell RF, Thapa P, Cheville JC, et al. Oncologic Outcomes for Patients with Residual Cancer at Cystectomy Following Neoadjuvant Chemotherapy: A Pathologic Stage-matched Analysis. Eur Urol. 2017;72(5):660-4.
5. Sjodahl G, Lauss M, Lovgren K, Chebil G, Gudjonsson S, Veerla S, et al. A molecular taxonomy for urothelial carcinoma. Clin Cancer Res. 2012;18(12):3377-86.
6. Cancer Genome Atlas Research N. Comprehensive molecular characterization of urothelial bladder carcinoma. Nature. 2014;507(7492):315-22.
7. Damrauer JS, Hoadley KA, Chism DD, Fan C, Tiganelli CJ, Wobker SE, et al. Intrinsic subtypes of high-grade bladder cancer reflect the hallmarks of breast cancer biology. Proc Natl Acad Sci U S A. 2014;111(8):3110-5.
8. Choi W, Porten S, Kim S, Willis D, Plimack ER, Hoffman-Censits J, et al. Identification of distinct basal and luminal subtypes of muscle-invasive bladder cancer with different sensitivities to frontline chemotherapy. Cancer Cell. 2014;25(2):152-65.
9. Kardos J, Chai S, Mose LE, Selitsky SR, Krishnan B, Saito R, et al. Claudin-low bladder tumors are immune infiltrated and actively immune suppressed. JCI Insight. 2016;1(3):e85902.
10. Sjodahl G, Eriksson P, Liedberg F, Hoglund M. Molecular classification of urothelial carcinoma: global mRNA classification versus tumour-cell phenotype classification. J Pathol. 2017;242(1):113-25.
11. Rosenberg JE, Hoffman-Censits J, Powles T, van der Heijden MS, Balar AV, Necchi A, et al. Atezolizumab in patients with locally advanced and metastatic urothelial carcinoma who have progressed following treatment with platinum-based chemotherapy: a single-arm, multicentre, phase 2 trial. Lancet. 2016;387(10031):1909-20.
12. Sharma P, Callahan MK, Bono P, Kim J, Spiliopoulou P, Calvo E, et al. Nivolumab monotherapy in recurrent metastatic urothelial carcinoma (CheckMate 032): a multicentre, open-label, two-stage, multi-arm, phase 1/2 trial. Lancet Oncol. 2016;17(11):1590-8.
13. Sharma P, Retz M, Siefker-Radtke A, Baron A, Necchi A, Bedke J, et al. Nivolumab in metastatic urothelial carcinoma after platinum therapy (CheckMate 275): a multicentre, single-arm, phase 2 trial. Lancet Oncol. 2017;18(3):312-22.
14. Seiler R, Ashab HAD, Erho N, van Rhijn BWG, Winters B, Douglas J, et al. Impact of Molecular Subtypes in Muscle-invasive Bladder Cancer on Predicting Response and Survival after Neoadjuvant Chemotherapy. Eur Urol. 2017;72(4):544-54.

15. Faltas BM, Prandi D, Tagawa ST, Molina AM, Nanus DM, Sternberg C, et al. Clonal evolution of chemotherapy-resistant urothelial carcinoma. Nat Genet. 2016;48(12):1490-9.
16. Erho N, Crisan A, Vergara IA, Mitra AP, Ghadessi M, Buerki C, et al. Discovery and validation of a prostate cancer genomic classifier that predicts early metastasis following radical prostatectomy. PLoS One. 2013;8(6):e66855.
17. Piccolo SR, Sun Y, Campbell JD, Lenburg ME, Bild AH, Johnson WE. A single-sample microarray normalization method to facilitate personalized-medicine workflows. Genomics. 2012;100(6):337-44.
18. Wilkerson MD, Hayes DN. ConsensusClusterPlus: a class discovery tool with confidence assessments and item tracking. Bioinformatics. 2010;26(12):1572-3.
19. Subramanian A, Tamayo P, Mootha VK, Mukherjee S, Ebert BL, Gillette MA, et al. Gene set enrichment analysis: a knowledge-based approach for interpreting genome-wide expression profiles. Proc Natl Acad Sci U S A. 2005;102(43):15545-50.
20. Charoentong P, Finotello F, Angelova M, Mayer C, Efremova M, Rieder D, et al. Pan-cancer Immunogenomic Analyses Reveal Genotype-Immunophenotype Relationships and Predictors of Response to Checkpoint Blockade. Cell Rep. 2017;18(1):248-62.
21. Fleischmann A, Thalmann GN, Perren A, Seiler R. Tumor regression grade of urothelial bladder cancer after neoadjuvant chemotherapy: a novel and successful strategy to predict survival. Am J Surg Pathol. 2014;38(3):325-32.
22. Korpal M, Puyang X, Jeremy Wu Z, Seiler R, Furman C, Oo HZ, et al. Evasion of immunosurveillance by genomic alterations of PPARgamma/RXRalpha in bladder cancer. Nat Commun. 2017;8(1):103.
23. Seiler R, Oo HZ, Tortora D, Clausen TM, Wang CK, Kumar G, et al. An Oncofetal Glycosaminoglycan Modification Provides Therapeutic Access to Cisplatin-resistant Bladder Cancer. Eur Urol. 2017;72(1):142-50.
24. Loi S, Dushyanthen S, Beavis PA, Salgado R, Denkert C, Savas P, et al. RAS/MAPK Activation Is Associated with Reduced Tumor-Infiltrating Lymphocytes in Triple-Negative Breast Cancer: Therapeutic Cooperation Between MEK and PD-1/PD-L1 Immune Checkpoint Inhibitors. Clin Cancer Res. 2016;22(6):1499-509.
25. Dadhania V, Zhang M, Zhang L, Bondaruk J, Majewski T, Siefker-Radtke A, et al. Meta-Analysis of the Luminal and Basal Subtypes of Bladder Cancer and the Identification of Signature Immunohistochemical Markers for Clinical Use. EBioMedicine. 2016;12:105-17.
26. Bracci L, Schiavoni G, Sistigu A, Belardelli F. Immune-based mechanisms of cytotoxic chemotherapy: implications for the design of novel and rationale-based combined treatments against cancer. Cell Death Differ. 2014;21(1):15-25.
27. Kurtova AV, Xiao J, Mo Q, Pazhanisamy S, Krasnow R, Lerner SP, et al. Blocking PGE2-induced tumour repopulation abrogates bladder cancer chemoresistance. Nature. 2015;517(7533):209-13.
28. Metcalfe M, Sundi D, Li R, Ferguson J, Shanna P, Jolanta B, et al. The effect of intrinsic subtype on response to neoadjuvant chemotherapy for muscle invasive bladder cancer. J Urol. 2017;197(4S):e1194.
29. Van Allen EM, Mouw KW, Kim P, Iyer G, Wagle N, Al-Ahmadie H, et al. Somatic ERCC2 mutations correlate with cisplatin sensitivity in muscle-invasive urothelial carcinoma. Cancer Discov. 2014;4(10):1140-53.
30. Plimack ER, Dunbrack RL, Brennan TA, Andrake MD, Zhou Y, Serebriiskii IG, et al. Defects in DNA Repair Genes Predict Response to Neoadjuvant Cisplatin-based Chemotherapy in Muscle-invasive Bladder Cancer. Eur Urol. 2015;68(6):959-67.
31. Bellmunt J, Kerst JM, Vazquez F, Morales-Barrera R, Grande E, Medina A, et al. A randomized phase II/III study of cabazitaxel versus vinflunine in metastatic or locally advanced transitional cell carcinoma of the urothelium (SECAVIN). Ann Oncol. 2017;28(7):1517-22.

32. Petrylak DP, de Wit R, Chi KN, Drakaki A, Sternberg CN, Nishiyama H, et al. Ramucirumab plus docetaxel versus placebo plus docetaxel in patients with locally advanced or metastatic urothelial carcinoma after platinum-based therapy (RANGE): a randomised, double-blind, phase 3 trial. Lancet. 2017;390(10109):2266-77.
33. Green DR. The end and after: how dying cells impact the living organism. Immunity. 2011;35(4):441-4.
34. Qian LW, Fourcaudot AB, Yamane K, You T, Chan RK, Leung KP. Exacerbated and prolonged inflammation impairs wound healing and increases scarring. Wound Repair Regen. 2016;24(1):26-34.
35. Nieto MA, Huang RY, Jackson RA, Thiery JP. Emt: 2016. Cell. 2016;166(1):21-45.
36. Dvorak HF. Tumors: wounds that do not heal-redux. Cancer Immunol Res. 2015;3(1):1-11.
37. Thomsen MBH, Nordentoft I, Lamy P, Vang S, Reinert L, Mapendano CK, et al. Comprehensive multiregional analysis of molecular heterogeneity in bladder cancer. Sci Rep. 2017;7(1):11702.
38. Lindgren D, Gudjonsson S, Jee KJ, Liedberg F, Aits S, Andersson A, et al. Recurrent and multiple bladder tumors show conserved expression profiles. BMC Cancer. 2008;8:183.
39. Smith SC, Baras AS, Dancik G, Ru Y, Ding KF, Moskaluk CA, et al. A 20-gene model for molecular nodal staging of bladder cancer: development and prospective assessment. Lancet Oncol. 2011;12(2):137-43.
40. Robertson AG, Kim J, Al-Ahmadie H, Bellmunt J, Guo G, Cherniack AD, et al. Comprehensive Molecular Characterization of Muscle-Invasive Bladder Cancer. Cell. 2017;171(3):540-56 e25.
41. Cesano A. nCounter((R)) PanCancer Immune Profiling Panel (NanoString Technologies, Inc., Seattle, WA). J Immunother Cancer. 2015;3:42.
42. Kanehisa M, Furumichi M, Tanabe M, Sato Y, Morishima K. KEGG: new perspectives on genomes, pathways, diseases and drugs. Nucleic Acids Res. 2017;45(D1):D353-D61.

FIGURE Legends

Figure 1: Molecular subtyping of pre-NAC TURBT and post-NAC RC bladder cancer samples using the GSC. (A) Prognosis using the GSC in the pre-NAC setting (n=114); (B) Prognosis using the GSC in the post-NAC setting (n=114); (C) Distribution of subtype calls in the pre-NAC and post-NAC setting (n=116); (D) Comparison of subtype calls using different models (n=116), samples are ordered according to the GSC model in both the pre- and post-NAC settings; (E) Concordance of models with respect to the basal / luminal axis (n=116), where complete model agreement is the darkest blue (or red) and scored as 5 (see Methods for additional details). The MDA p53-like and Lund Infiltrated subtypes have zero weighted votes. The grey box indicates a tie between the agreement of the models. The Fleiss' Kappa indicates the concordance across the different models and is significantly higher in pre-NAC when compared to the post-NAC samples.

Figure 2: Defining novel biological clusters using gene expression profiling in post-NAC bladder cancer. (A) Forced-order heatmap for selected MIBC marker genes (see text for description); (B) basal gene signature (14), (C) luminal gene signature (14), (D) IHC with KRT5/6 and GATA3 antibodies showing higher staining in CC1-Basal and CC2-Luminal tumors, respectively. (E) Summary of IHC staining across the TMA for KRT5/6 and CD44, (F) Summary of IHC staining across the TMA for GATA3 and PPARγ.

Figure 3: Enrichment of immune cells and immune signaling pathways in CC3-Immune. (A) Pan cancer immune gene enrichment signature (41); (B) A generalized immune signature (Immune190) (22); (C) T-cell gene signature (9); (D) T-helper cell gene signature (9); (E) IHC with anti-CD8 antibodies showing enrichment of T-cells; (F) summary of CD8 IHC across the entire TMA; (G) a gene enrichment signature for cytokines / chemokines (42).

Figure 4: Gene expression similarities between non-neoplastic scar-tissues and the CC4-Scar-like subtype from RC tumor specimens. (A) H&E stained sections; (B) IHC with KI67 antibodies; (C) summary of KI67 IHC across the entire TMA; (D) Cell cycle gene signature (9); (E) ECM gene signature (8); (F) median-fold change comparison of CC4 and scar tissue gene expression; (G) PCA on four consensus clusters with scar tissue – left panel / right panel; and (H) KM plot for overall survival.

Figure 5: Proposed model to describe plasticity in cisplatin-treated MIBC. (A) Apoptosis causes cytokine release and immune cell recruitment to tumor site; CC3-Immune, (B) Tumor does not respond to therapy and maintains subtype, (C) Tumor partially regresses and adopts a scar-like phenotype, (D) Tumor cells are mostly cleared but repopulated with a less differentiated cancer cell population (previously luminal becomes basal) or with a cell population that is induced down a luminal differentiation pathway (if previously basal). The left arm represents luminal-type tumors (shown in dark blue) and the right arm represents basal tumors (shown in red). The right panel shows the GSC subtype pre-NAC and the corresponding consensus cluster post-NAC. The CC1-Basal tumors are indicated by red color, CC2-Luminal by dark blue, CC3-Immune by green and CC4-Scar-like by yellow.

Figure 6: Scheme indicating the classes identified after NAC and their phenotype and biological characteristics.

Figure 1

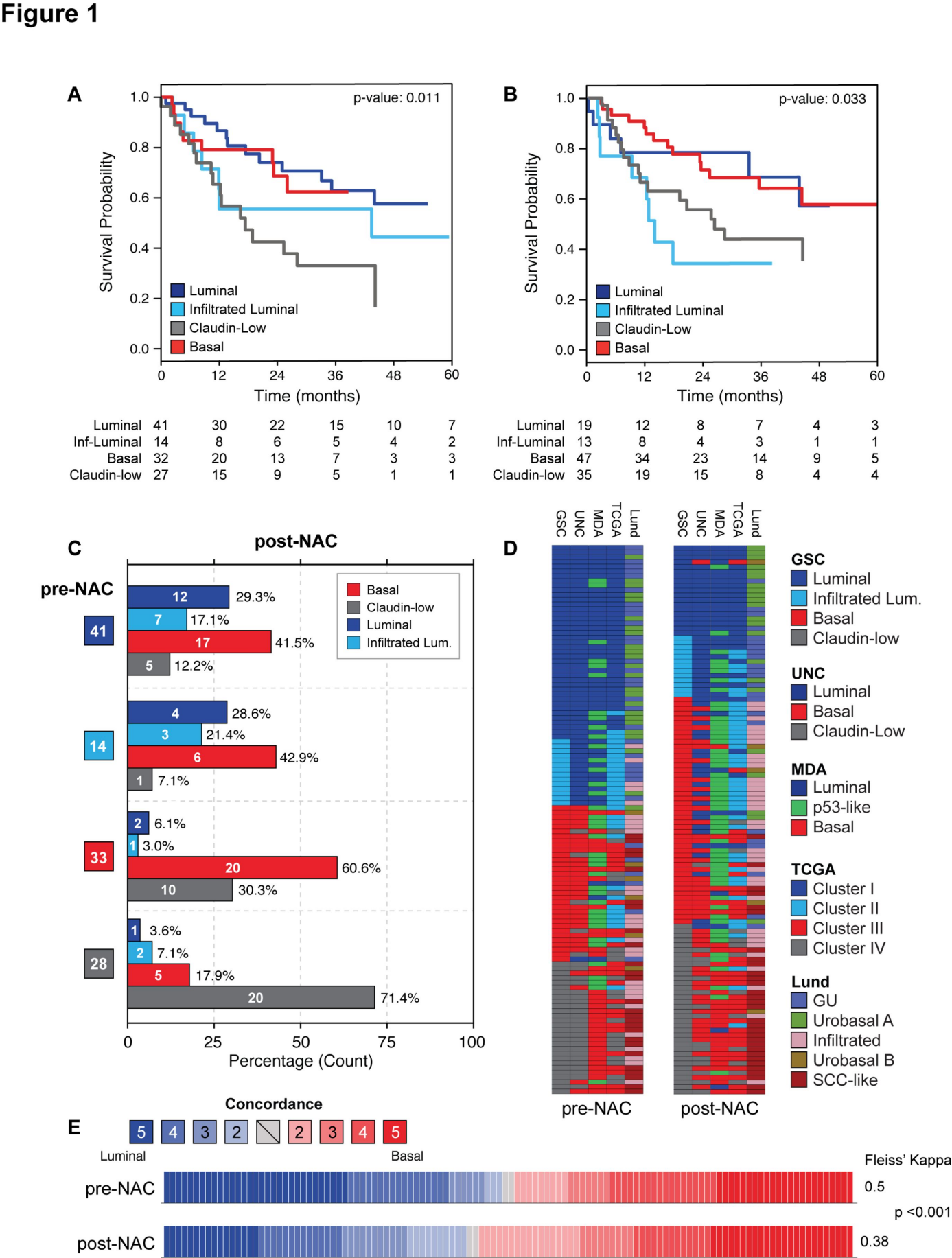
A
p-value: 0.011
Survival Probability
Time (months)
Luminal
Infiltrated Luminal
Claudin-Low
Basal
Luminal 41 30 22 15 10 7
Inf-Luminal 14 8 6 5 4 2
Basal 32 20 13 7 3 3
Claudin-low 27 15 9 5 1 1
B
p-value: 0.033
Survival Probability
Time (months)
Luminal
Infiltrated Luminal
Claudin-Low
Basal
Luminal 19 12 8 7 4 3
Inf-Luminal 13 8 4 3 1 1
Basal 47 34 23 14 9 5
Claudin-low 35 19 15 8 4 4
C
post-NAC
pre-NAC
Basal
Claudin-low
Luminal
Infiltrated Lum.
41
12 29.3%
7 17.1%
17 41.5%
5 12.2%
14
4 28.6%
3 21.4%
6 42.9%
1 7.1%
33
2 6.1%
1 3.0%
20 60.6%
10 30.3%
28
1 3.6%
2 7.1%
5 17.9%
20 71.4%
Percentage (Count)
D
GSC
UNC
MDA
TCGA
Lund
pre-NAC
post-NAC
GSC
Luminal
Infiltrated Lum.
Basal
Claudin-low
UNC
Luminal
Basal
Claudin-Low
MDA
Luminal
p53-like
Basal
TCGA
Cluster I
Cluster II
Cluster III
Cluster IV
Lund
GU
Urobasal A
Infiltrated
Urobasal B
SCC-like
E
Concordance
5 4 3 2 2 3 4 5
Luminal
Basal
pre-NAC
post-NAC
Fleiss' Kappa
0.5
p <0.001
0.38

Figure 2

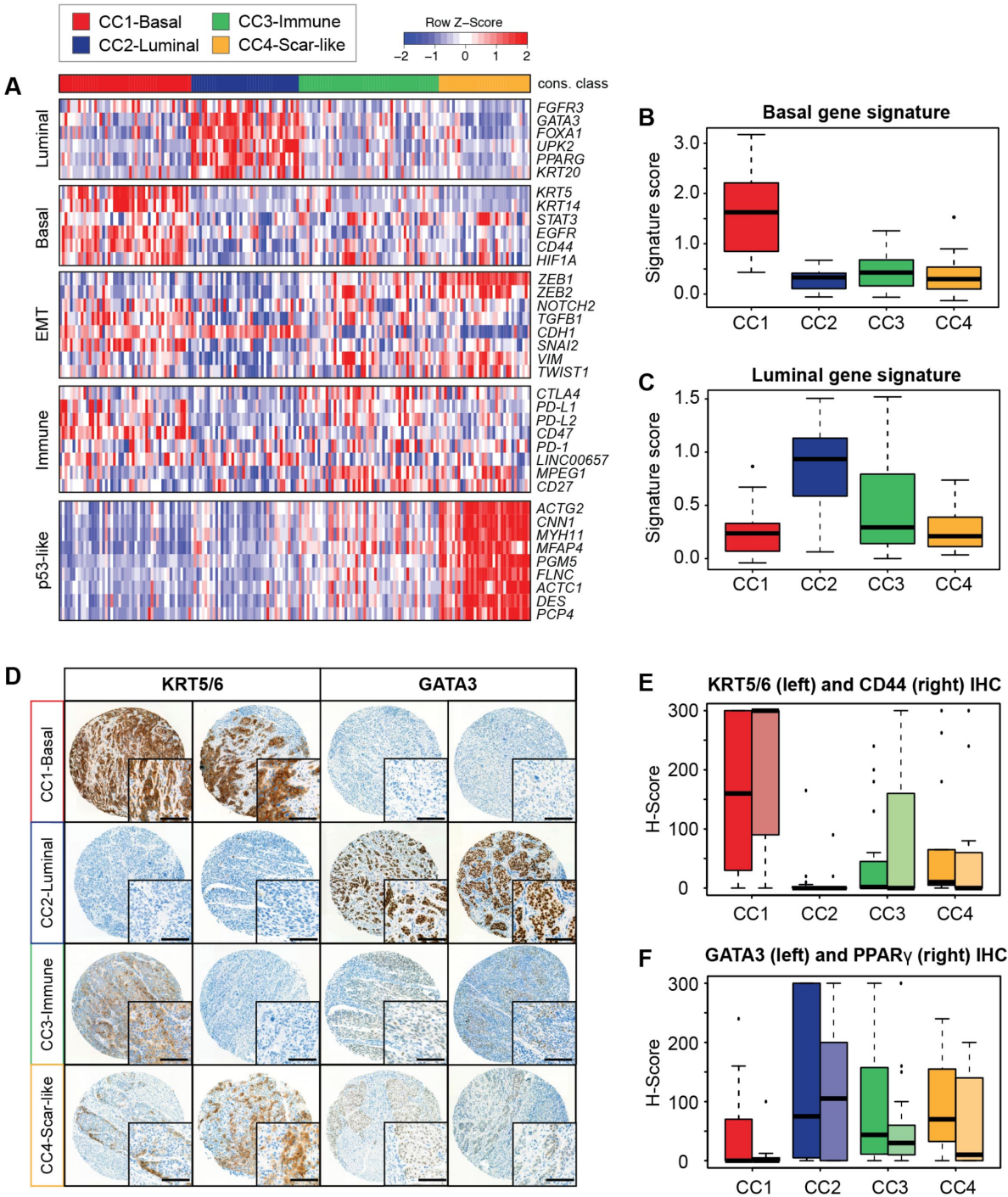
CC1-Basal
CC2-Luminal
CC3-Immune
CC4-Scar-like
Row Z-Score
−2 −1 0 1 2
A
cons. class
Luminal
FGFR3
GATA3
FOXA1
UPK2
PPARG
KRT20
Basal
KRT5
KRT14
STAT3
EGFR
CD44
HIF1A
EMT
ZEB1
ZEB2
NOTCH2
TGFB1
CDH1
SNAI2
VIM
TWIST1
Immune
CTLA4
PD-L1
PD-L2
CD47
PD-1
LINC00657
MPEG1
CD27
p53-like
ACTG2
CNN1
MYH11
MFAP4
PGM5
FLNC
ACTC1
DES
PCP4
B
Basal gene signature
Signature score
3.0
2.0
1.0
0.0
CC1
CC2
CC3
CC4
C
Luminal gene signature
Signature score
1.5
1.0
0.5
0.0
CC1
CC2
CC3
CC4
D
KRT5/6
GATA3
CC1-Basal
CC2-Luminal
CC3-Immune
CC4-Scar-like
E
KRT5/6 (left) and CD44 (right) IHC
H-Score
300
200
100
0
CC1
CC2
CC3
CC4
F
GATA3 (left) and PPARγ (right) IHC
H-Score
300
200
100
0
CC1
CC2
CC3
CC4

Figure 3

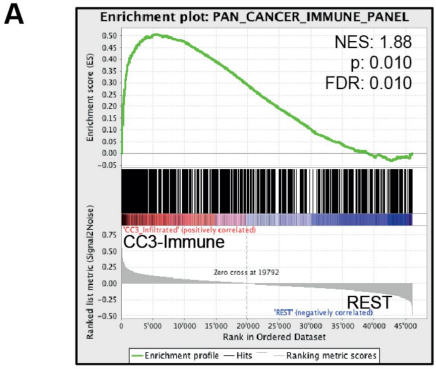
A
Enrichment plot: PAN_CANCER_IMMUNE_PANEL
NES: 1.88
p: 0.010
FDR: 0.010
Enrichment score (ES)
CC3-Immune
REST
Rank in Ordered Dataset
Enrichment profile
Hits
Ranking metric scores

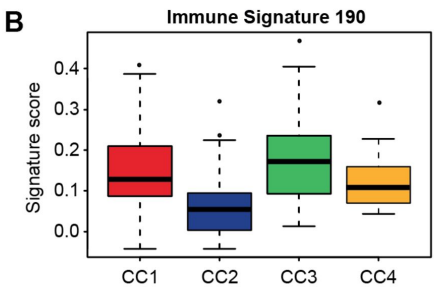
B
Immune Signature 190
Signature score
CC1
CC2
CC3
CC4

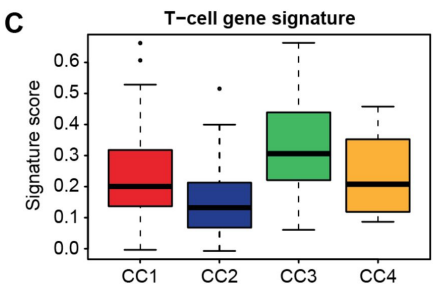
C
T−cell gene signature
Signature score
CC1
CC2
CC3
CC4

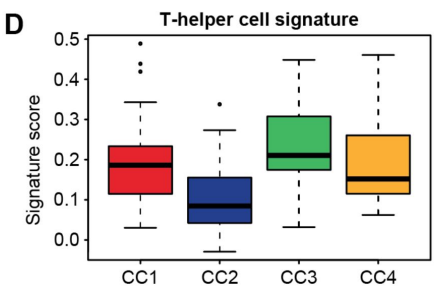
D
T-helper cell signature
Signature score
CC1
CC2
CC3
CC4

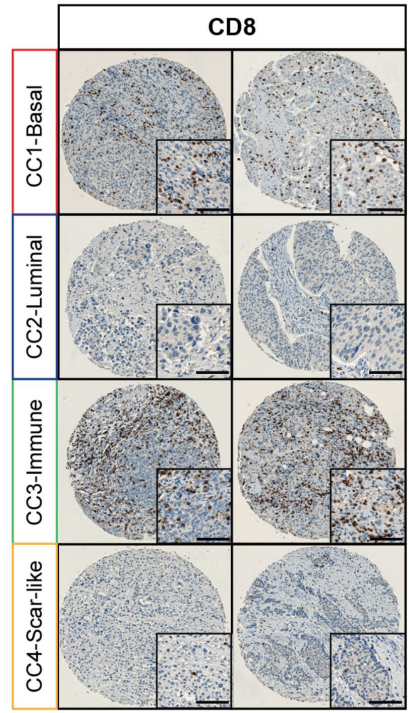
E
CD8
CC1-Basal
CC2-Luminal
CC3-Immune
CC4-Scar-like

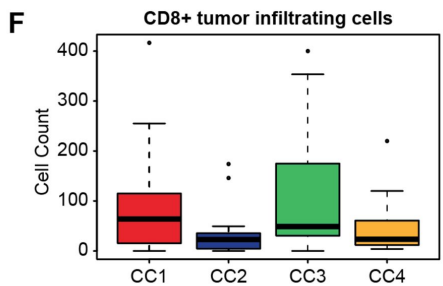
F
CD8+ tumor infiltrating cells
Cell Count
CC1
CC2
CC3
CC4

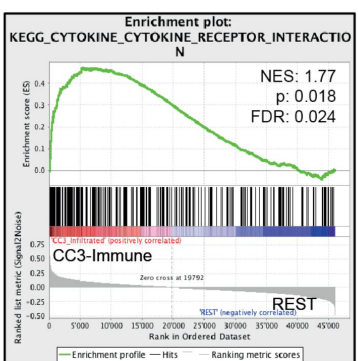
G
Enrichment plot:
KEGG_CYTOKINE_CYTOKINE_RECEPTOR_INTERACTIO
N
NES: 1.77
p: 0.018
FDR: 0.024
Enrichment score (ES)
CC3-Immune
REST
Rank in Ordered Dataset
Enrichment profile
Hits
Ranking metric scores

Figure 4

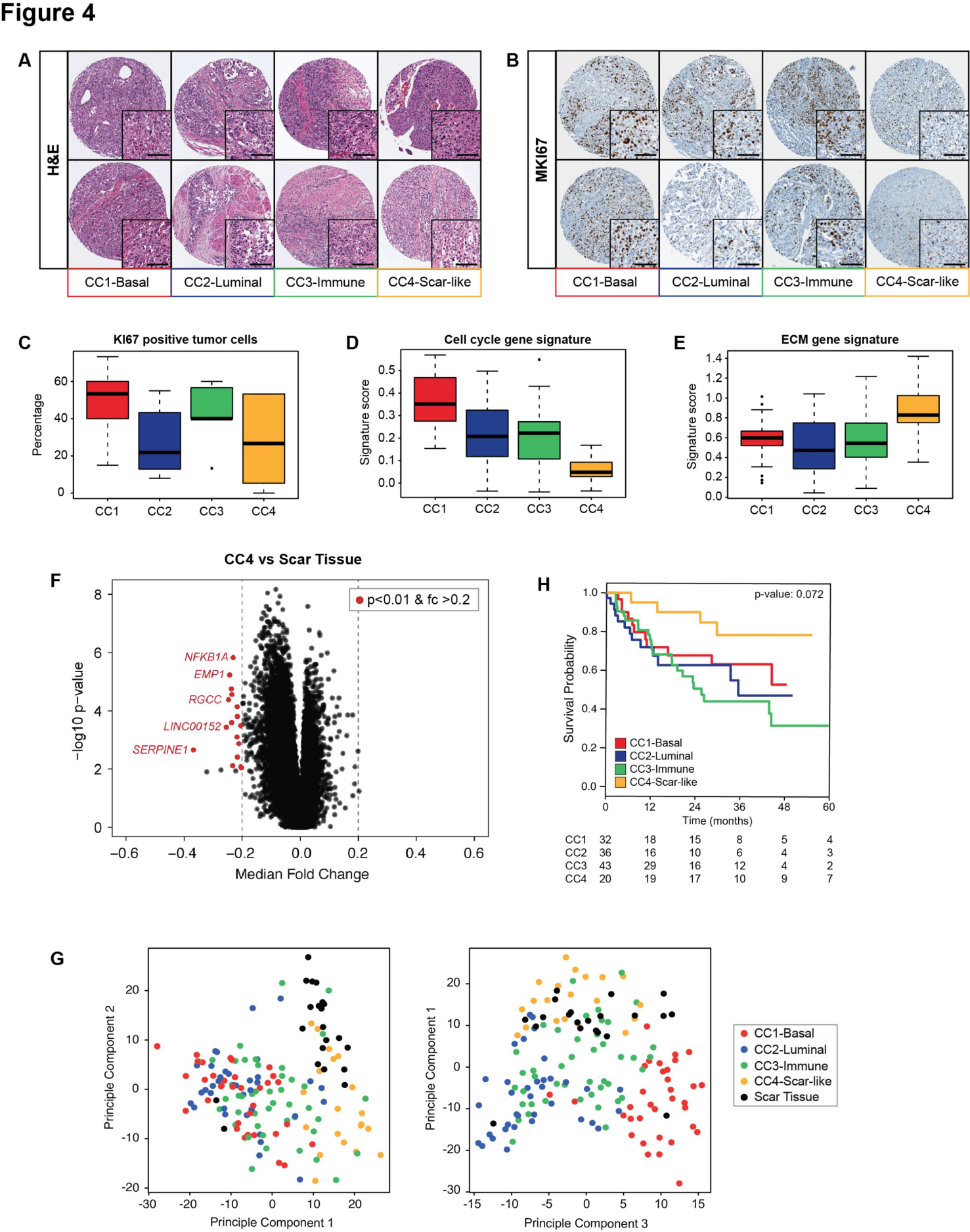
A
H&E
CC1-Basal
CC2-Luminal
CC3-Immune
CC4-Scar-like
B
MKI67
CC1-Basal
CC2-Luminal
CC3-Immune
CC4-Scar-like
C
KI67 positive tumor cells
Percentage
CC1
CC2
CC3
CC4
D
Cell cycle gene signature
Signature score
CC1
CC2
CC3
CC4
E
ECM gene signature
Signature score
CC1
CC2
CC3
CC4
F
CC4 vs Scar Tissue
p<0.01 & fc >0.2
NFKB1A
EMP1
RGCC
LINC00152
SERPINE1
−log10 p−value
Median Fold Change
H
p-value: 0.072
Survival Probability
CC1-Basal
CC2-Luminal
CC3-Immune
CC4-Scar-like
Time (months)
CC1 32 18 15 8 5 4
CC2 36 16 10 6 4 3
CC3 43 29 16 12 4 2
CC4 20 19 17 10 9 7
G
Principle Component 2
Principle Component 1
Principle Component 1
Principle Component 3
CC1-Basal
CC2-Luminal
CC3-Immune
CC4-Scar-like
Scar Tissue

Figure 5

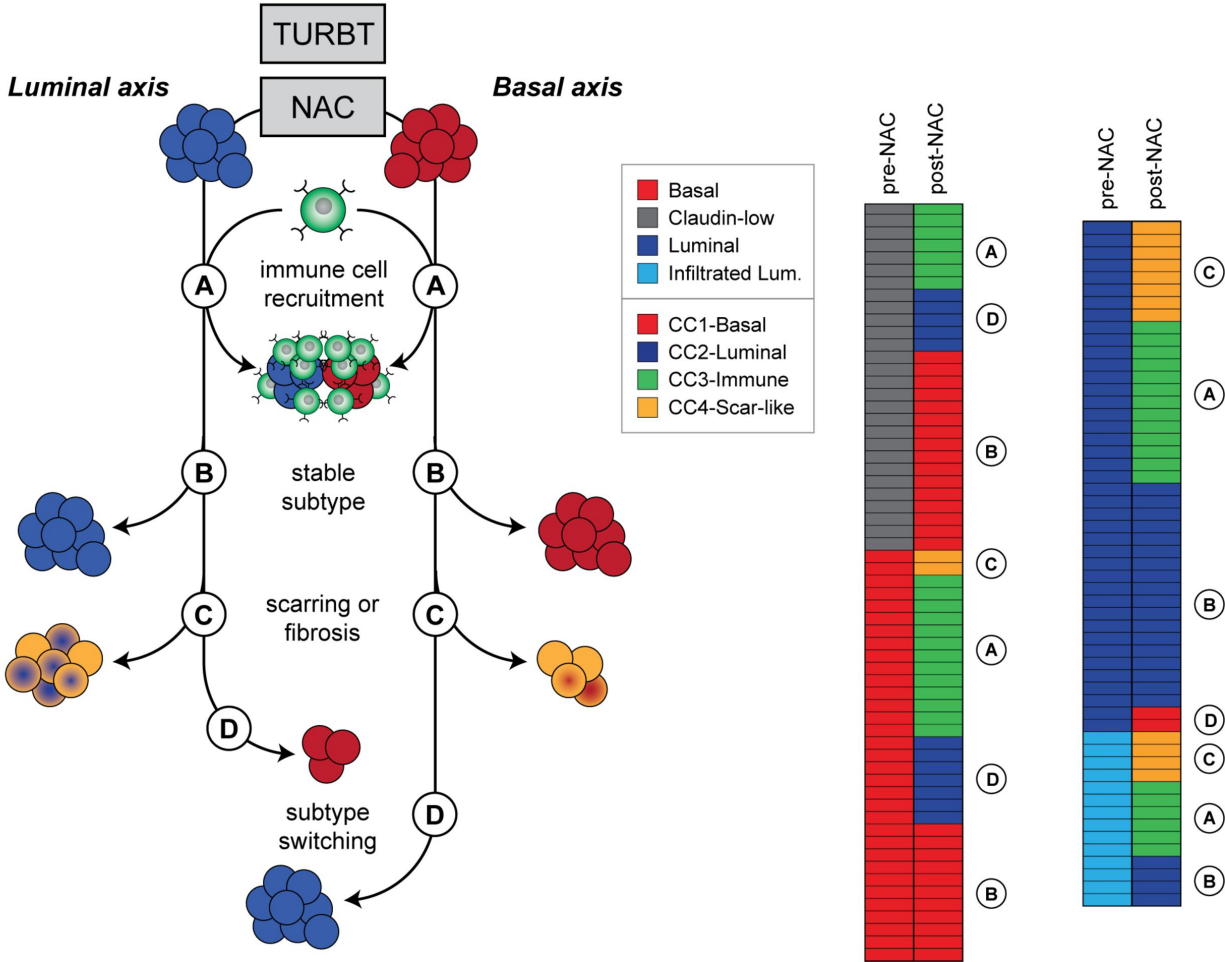
TURBT
NAC
Luminal axis
Basal axis
immune cell recruitment
stable subtype
scarring or fibrosis
subtype switching
A
B
C
D
Basal
Claudin-low
Luminal
Infiltrated Lum.
CC1-Basal
CC2-Luminal
CC3-Immune
CC4-Scar-like
pre-NAC
post-NAC
pre-NAC
post-NAC

Figure 6

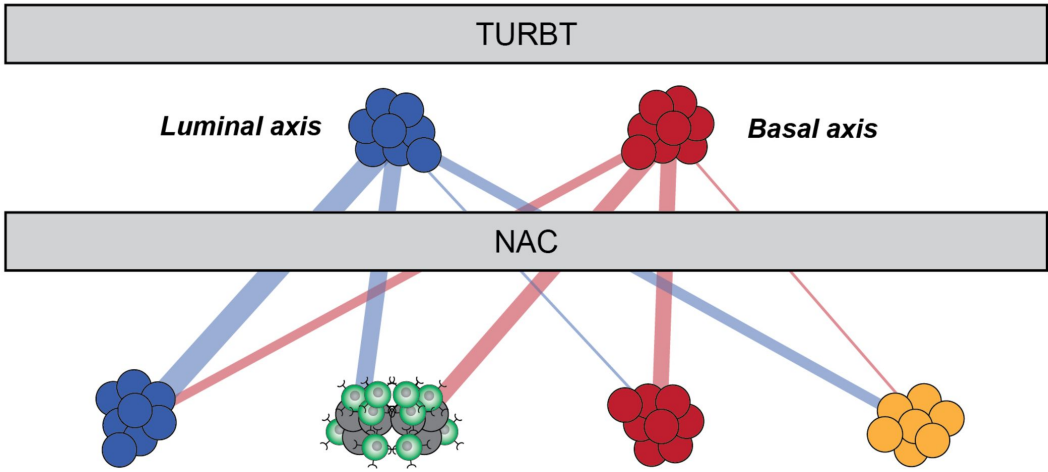

CC2-Luminal

Luminal-like phenotype
(GATA3+ / KRT5/6)
Low immune infiltration
Low proliferation

CC3-Immune

High immune infiltration
Strong immune genes
Weak cancer signals
Moderate proliferation

CC1-Basal

Basal-like phenotype
(KRT5/6+ & GATA3-)
Immune infiltrated
Highest proliferation

CC4-Scar-like

Stromal phenotype
Weak cancer signals
Low proliferation
Favorable prognosis